Published in final edited form as:
Neuroimage. 2010 January 15; 49(2): 1667–1676. doi:10.1016/j.neuroimage.2009.09.021.

3D mapping of somatotopic reorganization with small animal functional MRI

Xin Yu, **Shumin Wang**, **Der-Yow Chen**, **Stephen Dodd**, **Artem Goloshevsky**, and **Alan P. Koretsky**
National Institute of Neurological Disorders and Stroke, National Institutes of Health, Bethesda, MD, USA

Abstract

There are few *in vivo* noninvasive methods to study neuroplasticity in animal brains. Functional MRI (fMRI) has been developed for animal brain mapping, but few fMRI studies have analyzed functional alteration due to plasticity in animal models. One major limitation is that fMRI maps are characterized by statistical parametric mapping making the apparent boundary dependent on the statistical threshold used. Here, we developed a method to characterize the location of center-of-mass in fMRI maps that is shown not to be sensitive to statistical threshold. Utilizing centers-of-mass as anchor points to fit the spatial distribution of the BOLD response enabled quantitative group analysis of altered boundaries of functional somatosensory maps. This approach was used to study cortical reorganization in the rat primary somatosensory cortex (S1) after sensory deprivation to the barrel cortex by follicle ablation (F.A.). FMRI demonstrated an enlarged nose S1 representation in the 3D somatotopic functional maps. This result clearly demonstrates that fMRI enables the spatial mapping of functional changes that can characterize multiple regions of S1 cortex and still be sensitive to changes due to plasticity.

Introduction

Blood-oxygenation-level-dependent (BOLD) fMRI has been widely used for animal and human brain mapping (Bandettini et al., 1992; Kwong et al., 1992; Ogawa et al., 1992). As a noninvasive *in vivo* brain mapping approach, BOLD-fMRI and other fMRI techniques, such as perfusion-based cerebral blood flow (CBF) and contrast-based cerebral blood volume (CBV) methods, map hemodynamic changes due to neuronal activity in the brain (Kim and Tsekos, 1997; Rosen et al., 1991; Williams et al., 1992). A significant effort has been made to examine how well fMRI functional maps can localize brain activity in cortical subdivisions or columns (Kim et al., 2000; Yacoub et al., 2008). However, in all fMRI studies, the spatial extent of activity is defined at a given statistical threshold. Due to the large variability of statistical analysis among fMRI studies, no threshold setting standard is available. Indeed, numerous factors unrelated to neuronal activity can interfere with fMRI statistical analysis, such as the number of stimulation trials (Huettel and McCarthy, 2001), the signal-to-noise ratio of images (Saad et al., 2003), age-dependent physiological effects on hemodynamic response (Huettel et al., 2001), and the scanning acoustic background (Burke et al., 2000). In addition, BOLD

Address Correspondence to: Alan P. Koretsky LFMI, NINDS Building 10, Rm B1D728 10 Center Drive Bethesda, MD, 20892 koretskya@ninds.nih.gov Tel: 301-402-9659.

responses can vary greatly from different cortical regions due to region-specific hemodynamic response or different stimulation methods (Huettel et al., 2004; Inan et al., 2004). This makes it problematic to interpret functional maps of multiple cortical areas using a statistical threshold. Given the statistical aspect of fMRI, it is even more challenging to characterize the altered boundaries of functional maps in multiple cortical areas due to plasticity.

Mapping cortical reorganization with BOLD-fMRI has been reported in human and animal brains. In the human fMRI studies, altered brain function was mainly mapped in pathological or injured brains, such as language reorganization from epilepsy (Swanson et al., 2007), lesion-induced plasticity following traumatic brain injury and stroke (Hodics and Cohen, 2005; Levin, 2003), or cross-modal cortical reorganization in deaf or blind individuals (Finney et al., 2001; Sadato, 2006). There have been several fMRI studies of plasticity in rat models of stroke (Dijkhuizen et al., 2001), spinal cord injury (Endo et al., 2007), and peripheral denervation (Pelled et al., 2007; Sydekum et al., 2009). In all of these studies, changes of activity were measured by counting the number of active voxels at a given statistical threshold. Detailed alteration in spatial activity patterns has been seldom characterized, especially, during reorganization of adjacent cortices.

Cortical reorganization in the somatosensory cortex (S1) has been studied extensively with a variety of *in vivo* techniques. Electrophysiological recordings have demonstrated a conservative body representation in the S1 cortex across species, making the S1 cortex an excellent candidate to study cortical plasticity (Kaas et al., 1979; Mountcastle, 1957). Reorganization of S1 somatotopic maps have been analyzed by electrophysiology, voltage-sensitive dye imaging, and intrinsic signal optical imaging (Feldman and Brecht, 2005; Polley et al., 1999). In rat S1 fMRI studies, a number of different sensory stimuli have been applied to map individual S1 somatosensory areas (Sanganahalli et al., 2009), however, no study has mapped the S1 somatotopy and characterized the altered spatial patterns of activity in multiple adjacent cortices. Thus, the major goal of this study was to provide a method to map somatotopic organization and examine changes in the S1 cortex due to plasticity.

In the present work, BOLD-fMRI was performed on rats anesthetized with α-chloralose in an 11.7 Tesla MRI. Four subdivisions of the S1 cortex were mapped at 300 μm isotropic resolution using a three-dimensional (3D) gradient-echo echo planar imaging (EPI) sequence following electrical stimulation to the forepaw, hindpaw, whisker pads and nose. BOLD fMRI results showed that the size of the somatotopic functional maps varied largely depending on the statistical t-threshold used at the different S1 subdivisions, but the location of the center-of-mass (CM) in fMRI cortical maps was highly consistent regardless of t statistics used. The high consistency of the CM was also observed in S1 functional maps of rats with sensory deprivation in the barrel cortex by follicle ablation (F.A.) at postnatal day 10 (P10). Thus, the CM provides an excellent functional anchor point to fit the spatial pattern of BOLD response in 3D EPI images. The borders of functional maps in both control and F.A. rats were determined from a spatial fit of the BOLD response to analyze cortical organization and reorganization. To focus boundary detection on the cortical parenchyma, the BOLD signal from large vessels at the cortical surface were excluded from the spatial fitting. A significantly enlarged border-width for the S1 nose representation was observed in the F.A. rats. In addition, the 3D volumetric surface view demonstrated a clear expansion of the S1 nose representation toward the deprived barrel cortex in the F.A. rats. This confirmed the cortical reorganization established by electrophysiology (Waite and Taylor, 1978). Thus, this study mapped the somatotopic organization in the S1 cortex and visualized the 3D large-scale cortical reorganization throughout the rat brain. It is clear that BOLD-fMRI enables the spatial mapping of functional alteration over many somatosensory areas in a greater detail than other *in vivo* mapping techniques.

Materials and methods

Surgical preparations

Follicle ablation was performed at postnatal day 10 (P10) to remove whiskers from the whole whisker pad. After rat pups were anesthetized with Isofluorane, a slit was made in the whisker pad between row C and D using a small scalpel blade. Whisker follicles were removed by pulling the attached whiskers from underneath the skin flap with micro-dissecting tweezers. By separating the skin of the whisker pad from the underneath muscle, we could identify all follicles for removal. After whisker follicles were removed sterile swabs were used to remove any blood and to reposition the two edges of the slit by tissue glue. For those undergoing a sham procedure, incisions were made into the whisker pad, but no follicles were removed. Only male pups were chosen for this study. Rats were checked every other day for two weeks to ensure no missed follicles and for the regrowth of whiskers.

Animal preparation for functional MRI

Fifteen male *Sprague*-Dawley rats were imaged at 7-8 weeks of age. Nine of these rats had follicle ablation at P10 and six rats had a sham procedure at the same age. Rats were initially anesthetized with isoflurane. Each rat was orally intubated and placed on a mechanical ventilator throughout the surgery and the experiment. Plastic catheters were inserted into the right femoral artery and vein to allow monitoring of arterial blood gases and administration of drugs. After surgery, all animals were given i.v. bolus of α-chloralose (80mg/kg) and isoflurane was discontinued. Anesthesia was maintained with a constant α-chloralose infusion (26.5mg/kg/hr). The rats were placed on a heated water pad to maintain rectal temperature at ~37°C while in the magnet. Each animal was secured in a head holder with a bite bar to prevent head motion. End-tidal CO_2, rectal temperature, tidal pressure of ventilation, heart rate, and arterial blood pressure were continuously monitored during the experiment. Arterial blood gas levels were checked periodically and corrections were made by adjusting respiratory volume or administering sodium bicarbonate to maintain normal levels when required. An i.v. injection of pancuronium bromide (4 mg/kg) was given once per hour to reduce motion artifacts.

Somatosensory stimulation paradigm

To map the somatosensory cortex, needle electrodes were inserted just under the skin of different body parts, including forepaw, hindpaw, nose and whisker pad. A custom-made needle electrode pad was designed to deliver current across the whole whisker pad and the snout area. Because the locations of thewhisker pad and the nostril area are close to each other, the electrode was setup one at a time to ensure no cross-talk between electrodes. The current delivered to the whisker pad covers a large area (6×6 mm), which could spread to activate some of the face area, including the snout S1. This could contribute to a large overlap of the barrel cortex functional map with the nose S1 representation region (Fig 1). A World Precision Instruments stimulator (WPI, FL) supplied 2.5 mA, 300 μs pulses repeated at 3Hz to electrodes in the different body parts upon demand.

MRI image acquisition

All images were acquired with an 11.7 T/31 cm horizontal bore magnet (Magnex, Abingdon, UK), interfaced to an AVANCE III console (Bruker, Billerica, MA) and equipped with a 12 cm gradient set, capable of providing 100 G/cm with a rise time of 150μs (Resonance Research, MA). Shimming was performed with a custom-built shim set and high power shim supply (Resonance Research, MA). A custom-built 9 cm diameter transmitter coil was used for transmit and a 2 cm diameter surface coil was used for receive employing a transmit/receive decoupling device. A 3D gradient-echo, EPI sequence was used for the fMRI studies. Setup included shimming, adjustments to echo spacing and symmetry, and B_0 compensation. A single

shot sequence with a 64 × 64 × 32 matrix was run with the following parameters: effective echo time (TE) 16ms, repetition time (TR) 1.5s, bandwidth 200kHz, field of view 1.92 × 1.92 cm. This sequence gave isotropic resolution of 300 microns. The 3D slab was positioned to cover the S1 area of the animals. Block design stimulation paradigm was applied in this study. The paradigm consisted of 20 dummy scans to reach steady state, followed by 20 scans during rest, 20 scans during electrical stimulation, and 20 scans during rest, which was repeated 3 times (140 scans were acquired overall)., for a total experiment time of 3.5 min. The stimulation paradigm was repeated to acquire 7-9 multiple trials of a 3-epoch image set for each body part.

Imaging Processing and Statistical Analysis

fMRI data analysis was performed using Analysis of Functional NeuroImages (AFNI) software (NIH, Bethesda) (Cox, 1996). A series of AFNI routine function was applied to process the EPI image data (Supplementary notes). Statistical mapping produced a t-map to show the statistical significance of the linear regression analysis, and a beta map to estimate the amplitude of BOLD response. Before further image processing, the confounding BOLD signals contributed by large vessels on the cortical surface were first excluded. Voxels located at the cortical surface with BOLD signal mainly contributed from large vessels were filtered from data maps. These voxels were mainly distributed close to the midsagittal line, located medial and dorsal to the forepaw/hindpaw representation S1 areas.

To characterize the 3D spatial patterns of the somatotopic organization in the S1 cortex, image processing was performed with C and Matlab (Mathworks, MA) programming. First, 3D volumetric contour in the active S1 cortex was characterized from the t-map by setting an arbitrary t-threshold at 5. Amira software (Visage, CA) was applied for volumetric visualization. For visualization purposes only, an Amira built-in surface constraint function was utilized to smooth the 3D activity contours, and small clusters spreading in 3D space were excluded from visualization. All 3D contours for the active S1 subdivisions at both hemispheres were superimposed on the semi-transparent slab of rat brain. The voxel number and center of mass (CM) of the 3D contour were measured at different t-thresholds from 3 to the maximal value. The CM was calculated with the following equation:

$$\mathbf{R}_{\mathrm{CM(xcm,\ ycm,\ zcm)}} = \Sigma\left(\mathbf{r}_{\mathbf{i(xi,\ yi,\ zi)}}\mathbf{Xt_i}\right)/\Sigma\mathbf{t_i}$$

(r_i indicates the 3D coordinates of the voxel i, and t_i is the t value at the voxel i. Center of mass (R_{CM})is defined as the average of the positions, r_i, weighted by the t-value t_i)

The mean coordinate of CM was calculated by averaging individual CM coordinates at different t-thresholds. The distance between each individual CM to the mean CM was measured to examine the displacement of CMs at different t-thresholds. The spatial variability of CM was also demonstrated by assigning the standard deviation along the x, y and z axis to three radii of an ellipsoid whose center locates at the CM. Because a low t-threshold at 3 or 4 may include false-positive voxels due to multiple comparisons, the location of CM for each S1 subdivision was determined as the mean CM from t-threshold larger than 5. The p value at different t-threshold was calculated by AFNI (Supplementary Table 1)

The mean CM was used as the anchor point in the 3D space to model the spatial pattern of BOLD response in the beta map. The beta value of each voxel was derived from a linear regression analysis to estimate the amplitude of BOLD response (Cox, 1996), which is briefly described in the following equation:

$$\boldsymbol{Y_i} = \mathbf{X_i}\beta_\mathbf{i} + \varepsilon_\mathbf{i} \quad \mathbf{i} = 1, \ldots, \mathbf{n},$$

(Y_i are the measurements, X_i are the known regressors or predictor variables, β_i are the unknown parameters to be estimated for each voxel, ε_i are random errors.)

The parabolic profile of BOLD response along a line across two CMs was fitted with a second degree polynomial function. To better extrapolate the borders from the falling phase of the 1D spatial beta profile, the actual data included in the fitting process were first filtered by a linear extrapolation from a tangent line across the falling phase of the parabolic profile. This enabled the analysis of the major spatial component of positive BOLD response. The excluded spatial BOLD signal was considered as background noise. The standard deviation of the background noise was used to set a threshold to determine the data to be fitted (Supplementary Fig. 1A-C). Two roots of the parabolic fitting function were used to estimate the border-width of the BOLD response in active S1 subdivisions.

The reason that a second degree polynomial fitting was used was to extrapolate the borders along the falling phase of the 1D beta profile. The accuracy of the extrapolated border with the second degree polynomial fitting was evaluated with two other fitting methods: 1) tangent line extrapolation along the falling slope of the 1D beta profile; and 2) third degree polynomial fitting. The tangent line fitting only processes the points along the slope and the third degree polynomial fitting takes care of the asymmetry of the falling phase on both sides of the 1D profile and any negative spatial BOLD signal undershoot. The results of border-width estimated with all three fitting methods were the same as shown in the Supplementary Figure 2.

To create the 3D surface contour of the activated S1 subregions, polynomial fitting to the 1D beta profile of multiple lines across the CM in 3D space was applied. For each S1 subdivision, eighteen planes across the CM were determined in 3D space and eighteen lines at each plane were projected across the CM except for the line across two polar points (Fig. 5). A total 614 points were identified to estimate the border of the 3D spatial extent of the BOLD response (Supplementary Fig. 1D-F). Spherical topology mapping was applied to reconstruct the 3D activity contour using a triangular mesh. The final triangular surface mesh was constructed by connecting the 614 points with the same topology as if they were on a sphere. An averaged surface for each active S1 region was displayed for the two groups of rats (F.A. and Sham).

The triangular surface mesh and the CM point can be used to quantify the 3D volume of the activated S1 subregions. The 3D activated S1 area was divided into multiple tetrahedra (or triangular pyramid) by connecting the CM point and the three border points of each triangular mesh composing the 3D surface contour. Given the coordinates of the CM (C_i) and the three border points ($B1_i$, $B2_i$, $B3_i$) and a total of 1224 triangular meshes for each 3D surface contour, the volume of the 3D activated area was calculated with a dot product and cross product, yielding:

$$\bigvee = \Sigma\left(\left|\left(B1_i - \mathbf{C}_i\right) \cdot \left(B2_i - \mathbf{C}_i\right) \times \left(B3_i - \mathbf{C}_i\right)\right| / 6\right) \quad \mathbf{I} = 1, \ldots, \mathbf{n}, \ldots 1224$$

To compare the border-width and the 3D volume of activated S1 subregions between FA and Sham rats, a Student's t test (two-tail) was performed for group analysis, and the error bars in all graphs show the standard deviation.

Behavioral test

In order to test the effects of whisker removal on rats' exploratory behavior in a new environment, three groups of rats (SHAM: n=7, FA: n=7, Acute: n=5) were placed into a novel rectangle Plexiglas chamber (12×12×25 cm) for 5 min. The chamber was located inside a dark sound-attenuation cubicle. The exploratory behavior was recorded by an infrared camcorder.

The snout-touch behavior was defined when rats probed their snouts along and around surfaces of the wall or ceiling of the chamber explored during sniffing. Blind test was performed by two examiners when counting the snout-touch at the given time and the snout-touch count of each rat was averaged across examiners. The averaged snout-touch counts were analyzed by one-way ANOVA with a between-subject variable 'Group'. Post-hoc Scheffe test was used to examine the difference between groups.

Results

Somatotopic functional maps in the rat S1 cortex

To study cortical reorganization across the rat S1 area, it was necessary to first establish somatotopic functional maps with BOLD-fMRI. In this study, four S1 subdivisions were characterized for the representation of forepaw, hindpaw, nose and whisker pad (Fig. 1A, B). In four coronal EPI images across the different S1 subdivisions, 2D t-maps were superimposed on EPI images to represent the significant fMRI responses for the activated S1 subdivisions (Fig. 1C-F). BOLD signal time courses for each map demonstrated a good correlation with the stimulation paradigm (3 epochs of 30 s on/off block design). In addition, the fMRI functional maps were visualized as color-coded 3D contours in a segmented semi-transparent rat brain (Fig. 1B, Supplementary Movie 1), which agrees with the somatotopic maps established by electrophysiology (Chapin and Lin, 1984). The t-threshold was set at 5 to define the spatial pattern of the functional representation of each body part.

Functional mapping of multiple S1 areas at different t-thresholds

Although numerous studies have applied statistical thresholds to determine functional maps, it becomes problematic to quantify the borders of active S1 regions because these are highly dependent on the threshold used. Fig. 2A shows the spatial pattern of functional representation of forepaw, hindpaw, nose, and whisker pad at different t-thresholds. Clearly, the volumes of the active regions are significantly reduced with an increasing t-threshold. In addition, the profile of active volumes as a function of t-threshold varies across different S1 regions (Fig. 2B). Thus, it is difficult to define borders of functional maps of different S1 regions with a t-threshold because it is not clear which threshold should be used.

Since we acquired 3D images from the S1 area, the CM of functional maps could be characterized in each S1 subdivision. The location of the CM was highly consistent in functional maps regardless of the t statistics used to calculate the CM (Fig. 3). Only at the extremely high t-threshold ($t>20$) did the CM shift by only a few voxels. A mean CM coordinate was calculated by averaging the coordinates of CMs in functional maps defined at different t-thresholds. The spatial distribution of CMs was analyzed in the 3D space with a t-threshold up to 20. The displacement of CMs from the mean CM was plotted as a function of t-threshold, showing less than one voxel displacement for hindpaw and nose representation and less than 2 voxels for forepaw representation and the barrel cortex (Fig. 3). When a higher t-threshold was set, only a few active voxels with peak t values were highlighted in the functional maps. The CMs of these peak voxels shifted 2-3 voxels from the mean CM. The large shift was usually driven by separated hotspots of the S1 cortex, such as the multiple barrels in the barrel cortex or the dual representations of forepaw (Chapin and Lin, 1984). Despite the relatively large displacement from the CMs of peak voxels, the location of the mean CM was highly consistent across a large range of t-value used. Fig. 3C shows the spatial location of CMs in the 3D space. The small ellipsoid superimposed on each CM demonstrates the spatial variation of the CM at different t-thresholds.

The location of CMs in the F.A. rats was also determined in the BOLD functional maps. Since there is no whisker sensation following bilateral follicle ablation in the whisker pads, the

functional representations of forepaw, hindpaw, and nose were mapped in the F.A. rats with BOLD-fMRI. 2D t-maps and BOLD signal time course demonstrated well-preserved functional BOLD response in the three S1 subdivisions of F.A. rats (Fig. 4A-C). The CMs were measured in the functional maps of forepaw, hindpaw, and nose. Fig 4d displays the 3D location of CMs for both hemispheres. The spatial variation of the CMs at different t-thresholds is presented as the small ellipsoid superimposed on each CM in the 3D space. The location of the CM in F.A. rats showed less than 1-1.5 voxel shift from the mean CM at different t-threshold used (Fig. 4E-G). The highly consistent location of the CMs in both control and F.A. rats provides an excellent functional landmark for 3D functional mapping.

BOLD response beta-map modeling the spatial extent of S1 subdivision

The CMs provide accurate spatial locations of the functional maps to allow group analysis of spatial patterns of cortical activity among individual rats. In this experiment, the spatial pattern of the BOLD response in each S1 subdivision was analyzed using the 3D beta-map as has been done previously (Cox, 1996; Ford et al., 2005). The beta-map estimates the amplitude of BOLD response in each voxel of the 3D brain derived from the linear regression to the BOLD time courses. Using the CM as an anchor point in 3D space, the spatial distribution of BOLD signal in the beta map was determined in two consecutive steps. First, the BOLD response was measured on a line across any two CMs of the three S1 subdivisions and showed a typical parabolic spatial profile (Fig. 5A). A second degree polynomial curve fitting was applied to define the border of the BOLD response in active S1 regions along each line across the three CMs of forepaw, hindpaw, and nose representations (Fig. 5B). The border was calculated to estimate the spatial extent of the BOLD response. Group analysis showed a significantly expanded nose representation in both lines across nose-hindpaw and nose-forepaw CMs in the F.A. rats, while no difference was observed in the spatial representation of forepaw and hindpaw in the F.A. and control rats (Fig. 5C). This result indicated that only the S1 representation of nose was expanded in the F.A. rats.

In addition, two other fitting methods (tangent line border extrapolation and three degree polynomial fitting) were applied to examine the S1 cortical reorganization, showing similar values of the border-width to those estimated by the second degree polynomial fitting. In addition, a significantly expanded nose representation in the S1 was also observed by the other two fitting methods (Supplementary Figure 2). These results indicated that the second degree polynomial fitting is a reliable fitting method to extrapolate the border from the falling phase of the 1D beta profile.

The 1D spatial pattern of BOLD response determined between CMs can be extended to 3D space. Multiple lines across the CM were projected in all directions with 20 degrees rotation in each plane of 18 planes in the 3D space (See Materials and methods for detail). The 1D spatial profile of the BOLD response was fit to extrapolate the borders in each line. The estimated angular distance between borders of adjacent lines in the 3D space ranges from 1 to 1.5 voxel, i.e. 300 to 500μm. The volumetric active S1 region was constructed by mapping the extrapolated borders from all projected lines in 3D space. Here, the CMs provide a unique anchor point for the 3D functional mapping and enable the linear registration of functional maps from individual rat brains to the average CMs. After overlapping the estimated 3D volumetric activity maps, the nose representation was significantly enlarged in the F.A. rats compared to the sham control rats (Fig. 6, Supplementary Movie 2). In addition, the expansion is clearly toward the barrel cortex. The volume of the 3D surface contour was quantified, showing the volume of the S1 nose representation in the FA rats is more than two times larger than that in the SHAM rats. No significant volume difference was observed in the S1 FP/HP representation (detailed quantitative and statistical results are included in the Supplementary

Table 2). All together, these results provide a significant measure of the cortical reorganization in the nose S1 representation following deprivation of the barrel cortex.

Behavior associated with the fMRI measured cortical reorganization

To examine whether the enlarged nose S1 representation of the FA rats is formed in a use-dependent manner, the usage of nose was analyzed when rats explored a new environment. During normal exploratory behaviors, rats sample their surroundings by smell and whisker-touch. F.A. rats cannot whisk when exploring; therefore, sniffing and nose-poke have become the major components of exploratory behavior. Thus, a behavioral test was designed to count the snout-touch in the FA rats and SHAM rats with whisker or with whisker removed 12 hours before the test, a time when no signs of cortical plasticity occur in adult rodents(Welker et al., 1989). Blind analysis by two examiners showed a significantly higher number of snout-touches when the F.A. (153.38±25.77) and acute whisker removal (163.70±34.93) rats explored the new environment than the SHAM rats (103.71±19.11) with their whisker intact (Fig. 7, Supplementary Movie 3, 4, and 5). The number of snout-touches for FA rats increased over 48% and that for the acute whisker removal rats increased over 58%. This result indicates a use-dependent mechanism probably underlies the enlarged S1 cortical representation of the nostril area in the S1 cortex observed in the other nervous systems.

Discussion

In the present study, a 3D mapping approach was applied to analyze S1 cortical reorganization due to sensory deprivation in the barrel cortex. The spatial activity patterns of three S1 subdivisions surrounding the barrel cortex, *i.e.* the forepaw, hindpaw, and nose S1 representational zones, were measured using the 3D mapping approach, demonstrating an expanded nose representation toward the adjacent barrel cortex in F.A. rats. The enlarged nose map was correlated with an increased usage of snout when F.A. rats explored the new environment.

BOLD-fMRI mapping the spatial patterns of active S1 cortices

A key issue to determine the spatial extent of the BOLD response is to set a statistical threshold. Multiple comparisons of voxel-wise statistical mapping produce false-positive (type I) errors. Although several methods, such as Bonferroni correction, false discovery rate, or family-wise clustering, can be applied to adjust the threshold to exclude most false-positive errors, an increased number of active voxels can be improperly classified as inactive (type II error). The risk of error in either direction makes it difficult to have a standard threshold setting and leads to a large variability of the threshold used in most functional mapping studies. For example, in fMRI studies of the rat somatosensory cortex, t-test, cross-correlation analysis, etc. have all been used and at different thresholds. Thus, the lack of standard threshold setting in statistical parametric mapping makes it difficult to measure and compare cortical reorganization in fMRI maps. In the present study, functional maps of multiple S1 areas varied largely at different t-thresholds (Fig. 2), whereas the CMs of functional maps were highly consistent regardless of t-statistics. Thus, the CMs provide reliable functional landmarks to measure the spatial location of the boundary of functional maps. Several other rat fMRI studies have used CMs for the localization of forepaw and hindpaw activity maps (Duong et al., 2000;Endo et al., 2007;Spenger et al., 2000;Sydekum et al., 2009). Although the CMs in these studies were measured on a 2D activity map, the CM data in our study match the published values from these studies (Supplementary Table 3), which confirms the reliability of the location of CMs in functional maps.

Using the CM as an anchor point, the boundaries of the functional maps were determined by fitting the 1D spatial profile of the BOLD response in multiple lines projecting from the anchor

point in the beta map. Because the actual shape of the 1D spatial profile depends on the spatial location of the anchor point, it is necessary to apply a standard anchor point when analyzing the functional alteration between different groups of animals. In the present study, the CMs of functional maps are highly consistent across animal subjects and enable the group analysis of the spatial patterns of functional maps.

In the fitting process, a second degree polynomial curve was fitted to the major spatial component of the positive BOLD signal to extrapolate a border in 3D space. Occasionally, a minor spatial component of the positive BOLD and a negative spatial undershoot of BOLD signal appeared along the 1D spatial profile (Fig. 5). Previous studies have shown that a reliable minor BOLD spatial component could be detected in maps from rat brain with high signal-to-noise ratio obtained with a large number of EPI images (Goloshevsky et al., 2008). The secondary spatial component was observed in the overlap area between somatosensory representations. In the current study, 7-9 stimulation trials were repeated for each cutaneous periphery. Therefore, no attempt was made to extrapolate the border from fitting the minor spatial component in this study. Several tentative mechanisms may account for the small negative BOLD responses detected in the spatial profile, including a vascular origin due to a vascular blood “steal” effect by the active brain area, or a suppression of neuronal activity in the adjacent cortical area (Devor et al., 2005;Shmuel et al., 2006). The negative spatial BOLD signal was not included into the border fitting process. Use of a second degree polynomial was not intended to infer any specific model for the spatial extent of the BOLD response. Rather it was a fitting tool to extrapolate the border of the BOLD response from the falling edge of the BOLD response. A similar border was defined if a third degree polynomial or a simple line extrapolation was used (Supplementary Figure 2). This indicates that the extrapolated border is not highly dependent on the fitting procedure used.

In the future, EPI images with higher signal-to-noise ratio will be acquired to enable understanding and accounting for the spatial features of BOLD fMRI. In the present study, the 3D volumetric surface was generated by extrapolating the borders from the polynomial fit in all directions. It should be possible to improve the maps by following the cortical anatomy along layers to determine layer-specific CMs and the boundaries of cortical maps.

Comparison of electrophysiology map to BOLD-fMRI results

BOLD-fMRI maps of the body representation in the S1 cortex were in excellent agreement with the S1 cutaneous map established by single unit recording (Chapin and Lin, 1984). Both maps showed a similar trend of body representation with rostral cutaneous periphery in the medial S1 and caudal cutaneous periphery in the lateral S1, which has been observed in many species (Kaas et al., 1979; Mountcastle, 1957; Sur et al., 1978). In addition, the relative spatial location of body representations in the S1 cortex also agreed in the two maps. The distances between CMs in BOLD-fMRI maps (FP-HP: 2.09±0.38 mm; FP-Nose: 4.05±0.43 mm; HP-Nose: 4.44±0.27 mm) are similar to those obtained by electrophysiology maps (measured in Fig 3 of Ref. (Chapin and Lin, 1984), FP-HP: ~1.98 mm; FP-Nose: ~3 mm; HP-Nose: ~4.5 mm). The cortical reorganization in rats with whisker removal previously measured by electrophysiology is also similar to the BOLD-fMRI results obtained. Waite and Taylor (1978) reported cortical reorganization following removal of whiskers in young rats (Waite and Taylor, 1978). Electrophysiological recordings showed that the border of nose S1 close to the barrel cortex expanded 0.5-0.7 mm (measured in Fig 1 of Ref. (Waite and Taylor, 1978)) in the altered somatotopic maps. This agrees with the measurement of the expansion of the border of the nose S1 representational zone (0.546±0.18mm) in the BOLD-fMRI maps (Fig. 5). Moreover, BOLD-fMRI results provided a 3D volumetric surface view of the functional maps, clearly showing that the nose expansion was toward the barrel cortex and did not grow in all directions (Fig. 6, Supplementary Movie 2). This argues that lack of use of whisker barrels

and input into barrel cortex, along with increased use of nose was important for the cortical reorganization.

Some overlap was observed in the BOLD-fMRI functional maps between somatosensory areas that is not in the electrophysiological somatotopic map (Chapin and Lin, 1984). This may result from different neuronal mapping strategies of the two techniques. The electrophysiology map relies upon measuring a neuron's receptive field (RF) in the S1 cortex. A neuron's RF delimits the spatial range of the cutaneous periphery, where stimulation can induce a response. Although the RF can be of variable size, the center of the RF always indicates the preferred cutaneous periphery of the recorded neuron (Chapin and Lin, 1984). Thus, multiple recording sites sharing the same RF center can be grouped together, and different RF centers from the whole cutaneous periphery compose a topographic organization of neurons in the S1 cortex, i.e. the electrophysiological somatotopic map. Maps emerging from electrophysiological recordings usually reveal a clear border for the spatial distribution of neurons sharing the same RF centers. BOLD-fMRI maps the spatial pattern of blood flow, volume and oxygenation changes that are coupled to evoked neuronal activity due to stimulation at a given cutaneous periphery. Not only neurons with RF center located at the cutaneous periphery but also neurons whose RFs cover the cutaneous periphery can respond to the stimulation. In addition, it is not well established which types of neuronal activity can contribute to BOLD signal and it may be that sub-threshold activity in adjacent cortices elicit a BOLD response (Kim et al., 2004). Thus, stimulation of multiple peripheries can evoke activity in an ensemble of neurons with RF covering both peripheries and may result in the overlap of fMRI functional maps.

There are also numerous non-neuronal based factors that may contribute to and complicate the characterization of the spatial extent of fMRI functional maps, such as signal from draining veins (Disbrow et al., 2000; Ugurbil et al., 2003). In this study, we first excluded the confounding BOLD signals contributed by large vessels on the cortical surface. It is critical to remove surface vessel contributions from the functional maps because the high BOLD signal contributed by large surface vessels can bias the extrapolation of the border from the spatial pattern of the BOLD response(Keilholz et al., 2006).

To study the spatial aspect of neurovascular coupling, previous human fMRI studies measured a point-spread function (PSF) to estimate the spatial extent of the BOLD response from the neuronal activity source in the visual cortex (Engel et al., 1997; Parkes et al., 2005; Shmuel et al., 2007). The border of adjacent active visual areas was determined by differential analysis of the BOLD response to multiple visual stimuli. By analyzing the spatial distribution of the BOLD response across the estimated border, a full-width of half-maximal-height (FWHM) of Gaussian PSF was calculated to quantify the neurovascular spatial ranges from the activated neuronal loci. These have been reported to be from1.7 mm to 3.5 mm (Parkes et al., 2005). The large voxel size in human fMRI might overestimate the spatial extent of the BOLD response from close activity sources (Shmuel et al., 2007). In a high resolution (voxel size, 0.312×0.312×2 mm), perfusion-based fMRI study of orientation columns in the cat visual cortex, the FWHM of columnar clusters was estimated to be 470μm (Duong et al., 2001). Although the spatial specificity of the BOLD response is dependent on the voxel size, the positive BOLD signals were reported to be linearly correlated with the underlying neuronal activity at supra-millimeter spatial scales (Kim et al., 2004). Given the complicated nature of the neurovascular spatial correlation between the BOLD signal and actual locus of neuronal activity, we only focused on measuring the spatial patterns of the positive BOLD response to assess the S1 cortical reorganization. This approach does assume that an extrapolation of the border from the falling phase of the positive BOLD response leads to a proper boundary. Furthermore, the goodness of fit and the error of the boundary delimited will depend on the signal-to-noise ratio. In the present study using 300μm isotropic resolution, the half width of the overlap region between somatosensory areas, such as the forepaw and hindpaw S1 areas,

was between 300-400 m. Indeed, in each of the areas, the estimated PSF is nearly equal to the resolution used, indicating that the estimation may be determined by spatial resolution.

Mapping cortical reorganization in rats with BOLD-fMRI

There have been few fMRI studies of plasticity in the rat brain. Cortical reorganization in these studies was mainly analyzed by counting the number of active voxels at a given statistical threshold. Examples include increased BOLD fMRI in S1 of the contralateral non-affected body part following unilateral spinal cord injury or peripheral denervation (Pelled et al., 2007; Sydekum et al., 2009), and in the ipsilateral cortex following peripheral denervation (Pelled et al., 2007). In a rat model with complete transection of the mid-thoracic spinal cord, bilateral sensory deprivation of the hind limb led to an increased number of active pixels in the S1 cortex (Endo et al., 2007). In the present study, rather than focusing on a single S1 cortical area at an arbitrary statistical threshold, the 3D spatial patterns of S1 representations of forepaw, hindpaw and nose were estimated to analyze the cortical reorganization. This 3D mapping approach can be applied to study functional alterations of multiple cortices regardless of the statistical threshold.

The 3D volumetric surface view of the functional maps demonstrated the nose S1 representation enlarged preferentially towards the barrel cortex. No significant changes were observed in the forepaw and hindpaw S1 representational zones in the F.A. rats. Thus, the cortical reorganization in the sensory-deprived barrel cortex has a clear preference for the adjacent nose representational zone. Between the representation of paws and the barrel cortex is the central dysgranular zone (Chapin and Lin, 1984). This cytoarchitectural barrier may put the representation of paws at a disadvantage for expanding into the deprived barrel cortex. Besides the spatial arrangement of different S1 subdivisions, use-dependent plasticity can also contribute to the enlarged nose representational zones in the F.A. rats. The rat whisker system is inherently an active sensory system during exploratory behaviors. In this study, a gentle snout-touch to the explored area was often observed in F.A. and acute whisker removal rats to compensate for the lost whisker sweeping. The increased usage of nose as a peripheral sensational organ may drive the expansion of the nose representation to the deprived area in a use-dependent manner. In the future study, task related behavioral assays can be performed to test whether the enlarged representation affects the behavioral function of the nose, such as distinguishing the roughness/texture of a surface.

Supplementary Material

Refer to Web version on PubMed Central for supplementary material.

Acknowledgments

This research was supported by the Intramural Research Program of the NIH, NINDS. We thank Mss. Nadia Bouraoud and Kathy Sharer for their technical supports and animal surgery protocol preparation. We also thank Dr. David Leopold for his suggestions on the manuscript, and thank Drs. Daniel Glen, Ziad Saad, and Richard Reynolds for their help and support on image analysis with AFNI. We thank the assistance of the NIH Fellows Editorial Board for editing the manuscript.

Abbreviations

fMRI	functional magnetic resonance imaging
CM	center-of-mass
BOLD	blood oxygen level-dependent
S1	primary somatosensory cortex

CBF	cerebral blood flow
CBV	cerebral blood volume
RF	receptive field
PSF	point spread function

References

Bandettini PA, Wong EC, Hinks RS, Tikofsky RS, Hyde JS. Time course EPI of human brain function during task activation. Magn Reson Med 1992;25:390–397. [PubMed: 1614324]

Burke M, Schwindt W, Ludwig U, Hennig J, Hoehn M. Facilitation of electric forepaw stimulation-induced somatosensory activation in rats by additional acoustic stimulation: an fMRI investigation. Magn Reson Med 2000;44:317–321. [PubMed: 10918332]

Chapin JK, Lin CS. Mapping the body representation in the SI cortex of anesthetized and awake rats. J Comp Neurol 1984;229:199–213. [PubMed: 6438190]

Cox RW. AFNI: software for analysis and visualization of functional magnetic resonance neuroimages. Comput Biomed Res 1996;29:162–173. [PubMed: 8812068]

Devor A, Ulbert I, Dunn AK, Narayanan SN, Jones SR, Andermann ML, Boas DA, Dale AM. Coupling of the cortical hemodynamic response to cortical and thalamic neuronal activity. Proc Natl Acad Sci U S A 2005;102:3822–3827. [PubMed: 15734797]

Dijkhuizen RM, Ren J, Mandeville JB, Wu O, Ozdag FM, Moskowitz MA, Rosen BR, Finklestein SP. Functional magnetic resonance imaging of reorganization in rat brain after stroke. Proc Natl Acad Sci U S A 2001;98:12766–12771. [PubMed: 11606760]

Disbrow EA, Slutsky DA, Roberts TP, Krubitzer LA. Functional MRI at 1.5 tesla: a comparison of the blood oxygenation level-dependent signal and electrophysiology. Proc Natl Acad Sci U S A 2000;97:9718–9723. [PubMed: 10931954]

Duong TQ, Kim DS, Ugurbil K, Kim SG. Localized cerebral blood flow response at submillimeter columnar resolution. Proc Natl Acad Sci U S A 2001;98:10904–10909. [PubMed: 11526212]

Duong TQ, Silva AC, Lee SP, Kim SG. Functional MRI of calcium-dependent synaptic activity: cross correlation with CBF and BOLD measurements. Magn Reson Med 2000;43:383–392. [PubMed: 10725881]

Endo T, Spenger C, Tominaga T, Brene S, Olson L. Cortical sensory map rearrangement after spinal cord injury: fMRI responses linked to Nogo signalling. Brain 2007;130:2951–2961. [PubMed: 17913768]

Engel SA, Glover GH, Wandell BA. Retinotopic organization in human visual cortex and the spatial precision of functional MRI. Cereb Cortex 1997;7:181–192. [PubMed: 9087826]

Feldman DE, Brecht M. Map plasticity in somatosensory cortex. Science 2005;310:810–815. [PubMed: 16272113]

Finney EM, Fine I, Dobkins KR. Visual stimuli activate auditory cortex in the deaf. Nat Neurosci 2001;4:1171–1173. [PubMed: 11704763]

Ford JM, Johnson MB, Whitfield SL, Faustman WO, Mathalon DH. Delayed hemodynamic responses in schizophrenia. Neuroimage 2005;26:922–931. [PubMed: 15955502]

Goloshevsky AG, Dodd SJ, Koretsky AP. Assessment of Functional Cortical Plasticity with BOLD FMRI Mapping of Adjacent Somatosensory Representations in Rat. ISMRM 2008:2439.

Hodics T, Cohen LG. Functional neuroimaging in motor recovery after stroke. Top Stroke Rehabil 2005;12:15–21. [PubMed: 15940581]

Huettel SA, McCarthy G. The effects of single-trial averaging upon the spatial extent of fMRI activation. Neuroreport 2001;12:2411–2416. [PubMed: 11496120]

Huettel SA, Obembe OO, Song AW, Woldorff MG. The BOLD fMRI refractory effect is specific to stimulus attributes: evidence from a visual motion paradigm. Neuroimage 2004;23:402–408. [PubMed: 15325388]

Huettel SA, Singerman JD, McCarthy G. The effects of aging upon the hemodynamic response measured by functional MRI. Neuroimage 2001;13:161–175. [PubMed: 11133319]

Inan S, Mitchell T, Song A, Bizzell J, Belger A. Hemodynamic correlates of stimulus repetition in the visual and auditory cortices: an fMRI study. Neuroimage 2004;21:886–893. [PubMed: 15006655]

Kaas JH, Nelson RJ, Sur M, Lin CS, Merzenich MM. Multiple representations of the body within the primary somatosensory cortex of primates. Science 1979;204:521–523. [PubMed: 107591]

Keilholz SD, Silva AC, Raman M, Merkle H, Koretsky AP. BOLD and CBV-weighted functional magnetic resonance imaging of the rat somatosensory system. Magn Reson Med 2006;55:316–324. [PubMed: 16372281]

Kim DS, Duong TQ, Kim SG. High-resolution mapping of iso-orientation columns by fMRI. Nat Neurosci 2000;3:164–169. [PubMed: 10649572]

Kim DS, Ronen I, Olman C, Kim SG, Ugurbil K, Toth LJ. Spatial relationship between neuronal activity and BOLD functional MRI. Neuroimage 2004;21:876–885. [PubMed: 15006654]

Kim SG, Tsekos NV. Perfusion imaging by a flow-sensitive alternating inversion recovery (FAIR) technique: application to functional brain imaging. Magn Reson Med 1997;37:425–435. [PubMed: 9055234]

Kwong KK, Belliveau JW, Chesler DA, Goldberg IE, Weisskoff RM, Poncelet BP, Kennedy DN, Hoppel BE, Cohen MS, Turner R, et al. Dynamic magnetic resonance imaging of human brain activity during primary sensory stimulation. Proc Natl Acad Sci U S A 1992;89:5675–5679. [PubMed: 1608978]

Levin HS. Neuroplasticity following non-penetrating traumatic brain injury. Brain Inj 2003;17:665–674. [PubMed: 12850951]

Mountcastle VB. Modality and topographic properties of single neurons of cat's somatic sensory cortex. J Neurophysiol 1957;20:408–434. [PubMed: 13439410]

Ogawa S, Tank DW, Menon R, Ellermann JM, Kim SG, Merkle H, Ugurbil K. Intrinsic signal changes accompanying sensory stimulation: functional brain mapping with magnetic resonance imaging. Proc Natl Acad Sci U S A 1992;89:5951–5955. [PubMed: 1631079]

Parkes LM, Schwarzbach JV, Bouts AA, Deckers RH, Pullens P, Kerskens CM, Norris DG. Quantifying the spatial resolution of the gradient echo and spin echo BOLD response at 3 Tesla. Magn Reson Med 2005;54:1465–1472. [PubMed: 16276507]

Pelled G, Chuang KH, Dodd SJ, Koretsky AP. Functional MRI detection of bilateral cortical reorganization in the rodent brain following peripheral nerve deafferentation. Neuroimage 2007;37:262–273. [PubMed: 17544301]

Polley DB, Chen-Bee CH, Frostig RD. Varying the degree of single-whisker stimulation differentially affects phases of intrinsic signals in rat barrel cortex. J Neurophysiol 1999;81:692–701. [PubMed: 10036270]

Rosen BR, Belliveau JW, Buchbinder BR, McKinstry RC, Porkka LM, Kennedy DN, Neuder MS, Fisel CR, Aronen HJ, Kwong KK, et al. Contrast agents and cerebral hemodynamics. Magn Reson Med 1991;19:285–292. [PubMed: 1881317]

Saad ZS, Ropella KM, DeYoe EA, Bandettini PA. The spatial extent of the BOLD response. Neuroimage 2003;19:132–144. [PubMed: 12781733]

Sadato N. Cross-modal plasticity in the blind revealed by functional neuroimaging. Suppl Clin Neurophysiol 2006;59:75–79. [PubMed: 16893096]

Sanganahalli BG, Bailey CJ, Herman P, Hyder F. Tactile and non-tactile sensory paradigms for fMRI and neurophysiologic studies in rodents. Methods Mol Biol 2009;489:213–242. [PubMed: 18839094]

Shmuel A, Augath M, Oeltermann A, Logothetis NK. Negative functional MRI response correlates with decreases in neuronal activity in monkey visual area V1. Nat Neurosci 2006;9:569–577. [PubMed: 16547508]

Shmuel A, Yacoub E, Chaimow D, Logothetis NK, Ugurbil K. Spatio-temporal point-spread function of fMRI signal in human gray matter at 7 Tesla. Neuroimage 2007;35:539–552. [PubMed: 17306989]

Spenger C, Josephson A, Klason T, Hoehn M, Schwindt W, Ingvar M, Olson L. Functional MRI at 4.7 tesla of the rat brain during electric stimulation of forepaw, hindpaw, or tail in single- and multislice experiments. Exp Neurol 2000;166:246–253. [PubMed: 11085890]

Sur M, Nelson RJ, Kaas JH. The representation of the body surface in somatosensory area I of the grey squirrel. J Comp Neurol 1978;179:425–449. [PubMed: 417097]

Swanson SJ, Sabsevitz DS, Hammeke TA, Binder JR. Functional magnetic resonance imaging of language in epilepsy. Neuropsychol Rev 2007;17:491–504. [PubMed: 18058239]

Sydekum E, Baltes C, Ghosh A, Mueggler T, Schwab ME, Rudin M. Functional reorganization in rat somatosensory cortex assessed by fMRI: elastic image registration based on structural landmarks in fMRI images and application to spinal cord injured rats. Neuroimage 2009;44:1345–1354. [PubMed: 19015037]

Ugurbil K, Toth L, Kim DS. How accurate is magnetic resonance imaging of brain function? Trends Neurosci 2003;26:108–114. [PubMed: 12536134]

Waite PM, Taylor PK. Removal of whiskers in young rats causes functional changes in cerebral cortex. Nature 1978;274:600–602. [PubMed: 672993]

Welker E, Soriano E, Van der Loos H. Plasticity in the barrel cortex of the adult mouse: effects of peripheral deprivation on GAD-immunoreactivity. Exp Brain Res 1989;74:441–452. [PubMed: 2707320]

Williams DS, Detre JA, Leigh JS, Koretsky AP. Magnetic resonance imaging of perfusion using spin inversion of arterial water. Proc Natl Acad Sci U S A 1992;89:212–216. [PubMed: 1729691]

Yacoub E, Harel N, Ugurbil K. High-field fMRI unveils orientation columns in humans. Proc Natl Acad Sci U S A 2008;105:10607–10612. [PubMed: 18641121]

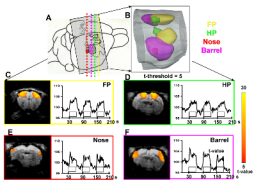

Figure 1. Somatotopic functional maps in the rat S1 cortex

Activated S1 areas after electrical stimulation of forepaw (FP, yellow), hindpaw (HP, green), whisker pad (Barrel, purple), and nose (Nose, red) are represented in 3D contour (**B**) and 2D coronal t-maps (**C-F**). The established S1 somatotopic map (**A**) matches 3D functional contours of the four body parts (**B**). Four 2D slices were selected across the four S1 subdivisions (**A**). Coronal 2D t maps (**C-F**, left panel) are shown with the time course of BOLD signal changes (**C-F**, right panel) in each S1 subdivision. The BOLD signal was normalized to baseline as 100.

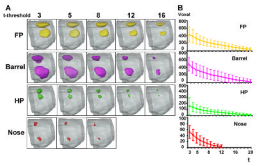

Figure 2. T-threshold dependent spatial patterns of S1 functional maps

The 3D contour of S1 representations of forepaw (FP, yellow), whisker pad (Barrel, purple), hindpaw (HP, green), and nose (Nose, red) are displayed at different t-threshold (**a**). The active voxel number is displayed as a function of t-threshold (**b**). The error bar demonstrates the standard deviation (SD) of active voxel numbers counted from all six rats.

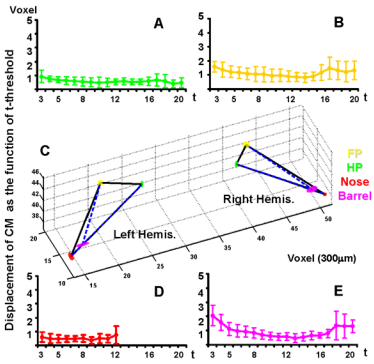

Figure 3. Localization of CMs in the 3D S1 somatotopic map

CMs of forepaw (FP, yellow), hindpaw (HP, green), whisker pad (Barrel, purple) and nose (Nose, red) S1 areas are shown at different t thresholds. The displacement from the CM determined at a given t-threshold to the mean CM is shown as a function of t-threshold (**A, B, D, and E**). Four CMs at both hemispheres are shown in 3D space with a transparent ellipsoid superimposed on each center, of which the three radii demonstrated the variability of the CM coordinates in x, y, and z axes (**C**).

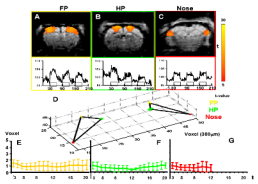

Figure 4. Somatotopic functional mapping in the S1 cortex of F.A. rats

S1 representations of forepaw, hindpaw, and nose are demonstrated in the 2D t-maps (**A-C**, upper panel). The BOLD signal time course demonstrated a well-preserved functional BOLD response in F.A. rats (**A-C**, lower panel). The location of CMs is represented in 3D space (**D**). A transparent ellipsoid was superimposed on each CM, of which the three radii demonstrated the variability of the CM coordinates along the x, y, and z axes. The displacement from the CM at a given t-threshold to the mean CM is shown as the function of t-threshold in the functional map of FP, HP, and Nose (**E-G**).

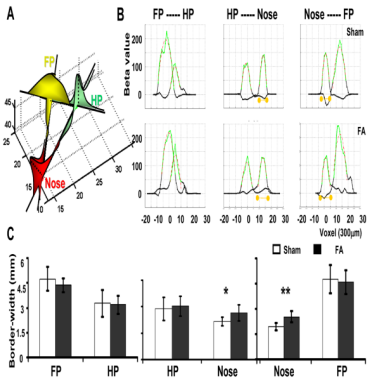

Figure 5. Analysis of the 1D spatial profile of BOLD response along lines across CMs

Three lines cross CMs of forepaw, hindpaw, and nose are demonstrated in the schematic graph (**A**). The beta value of each voxel along the line was plotted as a function of space in the 1D profile (**B**). Two lines were projected from each CM, and a total of six 1D spatial profiles were analyzed (**A**, FP, yellow; HP, green; nose, red). The filtered 1D spatial profile (green) was fitted by a second-order polynomial curve (red) for each line (**B**). The border-width from the extrapolated borders (**B**, orange dots) along each line was calculated to estimate the spatial extent of the BOLD response. A significantly expanded BOLD response in the S1 representation of nose in F.A. rats is shown (**C**). (* means p = 0.01;** p = 0.002; two tail, $N_{SHAM} = 6$, $N_{F.A.} = 9$).

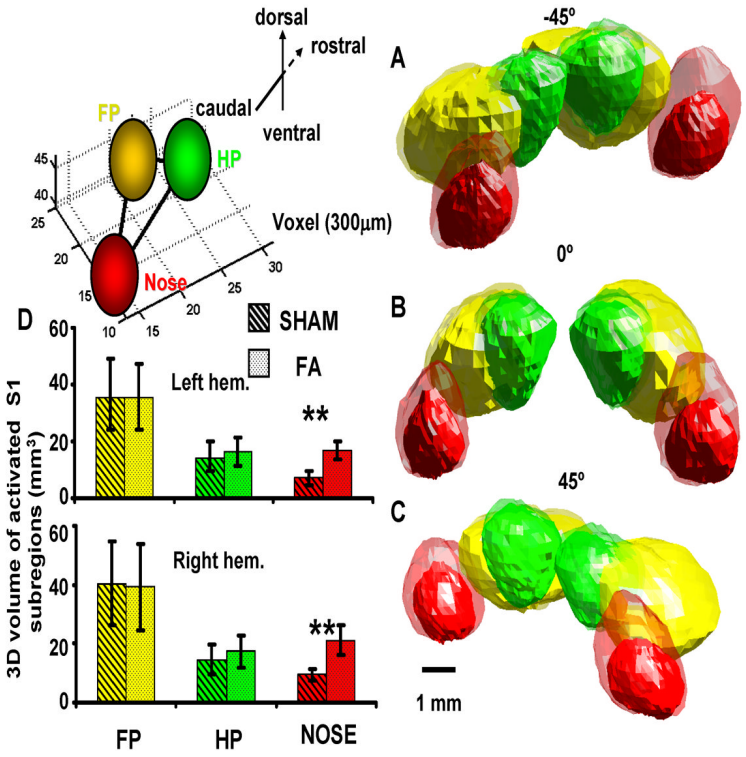

Figure 6. 3D volumetric estimation of the spatial pattern of BOLD response

The averaged 3D volumetric surface was displayed in 3D space to represent the S1 areas of forepaw (FP, yellow), hindpaw (HP, green), and nose (red) for both hemispheres (Sham, in solid color; F.A., in semi-transparent color). The left inset demonstrates the relative 3D location of the 3D volumetric contour. The superimposed 3D volumetric surfaces are displayed through a projection view at three angles (**A**-**C**; −45, 0, and 45). The quantitative results show a significantly larger 3D volume of the activated nose S1 representation of the FA rats than that of the SHAM rats (D; Student's t test: left, ** means p=0.0001; right **means p=0.0002).

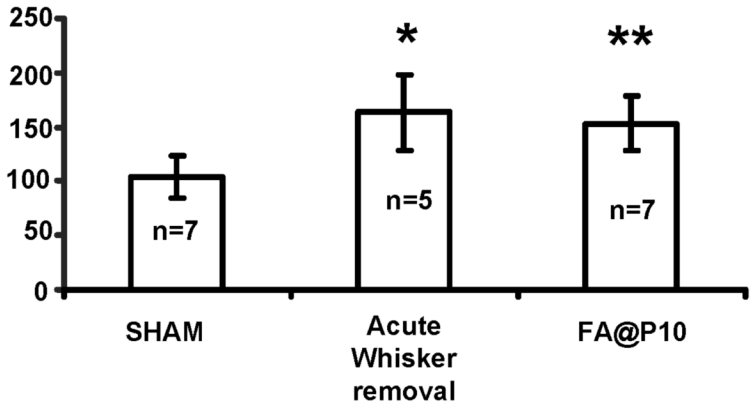

Figure 7. Environmental exploratory snout-touch for F.A. rats

The number of snout-touch was counted when sham, acute whisker removal, and F.A. rats were put into a new environment (**A**). Results of one-way ANOVA analysis show a significant group effect ($F(2,16) = 9.11$, $p = 0.002$). Post-hoc Scheffe test revealed that both Acute whisker removal and F.A. rats have more snout-touch counts than SHAM rats (*$p = 0.015$ and **0.005, respectively), but no significant difference between the Acute whisker removal and F.A. rats.